pH-controllable synthesis of unique nanostructured tungsten oxide aerogel and its sensitive glucose biosensor

2015 Nanotechnology 26 115602

(http://iopscience.iop.org/0957-4484/26/11/115602)

IOP Publishing Nanotechnology
Nanotechnology **26** (2015) 115602 (7pp) doi:10.1088/0957-4484/26/11/115602

pH-controllable synthesis of unique nanostructured tungsten oxide aerogel and its sensitive glucose biosensor

Qiang-Qiang Sun, Maowen Xu, Shu-Juan Bao and Chang Ming Li

Institute for Clean Energy & Advanced Materials, Faculty of Materials and Energy, Southwest University, Chongqing, 400715, People's Republic of China

E-mail: baoshj@swu.edu.cn

Received 16 September 2014, revised 29 January 2015
Accepted for publication 29 January 2015
Published 23 February 2015

Abstract

This work presents a controllable synthesis of nanowire-networked tungsten oxide aerogels, which was performed by varying the pH in a polyethyleneimine (PEI)-assisted hydrothermal process. An enzyme–tungsten oxide aerogel co-modified electrode shows high activity and selectivity toward glucose oxidation, thus holding great promise for applications in bioelectronics.

S Online supplementary data available from stacks.iop.org/NANO/26/115602/mmedia

Keywords: tungsten oxide, aerogel, biosensor

(Some figures may appear in colour only in the online journal)

1. Introduction

Tungsten oxides, in particular transition metal oxides, are of great interest and have been investigated extensively due to their promising physical and chemical properties. With outstanding electrochromic, optochromic, and gaschromic properties, tungsten oxides have been used to construct flat-panel displays, photoelectrochromic 'smart' windows, optical modulation devices, write–read–erase optical devices, and so forth [1–4]. Interest in WO_x can be traced to the seventeenth century, when the properties of $LiWO_3$ and techniques for WO_3 and $NaWO_3$ synthesis were first studied [5]. More recently, renewed research interest in WO_x was sparked by the advent of nanotechnology.

It is well known that nanomaterials are governed by a multitude of properties, such as structure, surface and textural characteristics, dimensions and morphology, and pore size distribution [6]. Therefore, controlling synthesis of materials is always one of the most challenging issues for inorganic chemists and material specialists. The ability to manage such a difficult task provides opportunities to reveal the relationships between material structures and properties and to aid the exploration of material fabrication techniques as well as novel applications of advanced nanostructures. Three-dimensional (3D) nanostructured aerogels have been the focus of a great deal of research due to their combination of feasible properties, which include extremely low density, low mean free path of diffusion, high specific surface area, low dielectric constant, and slow speed of sound. These aerogels have been used as a trapping medium for chemical analyses, especially for catalytic and electrochemical applications [7–9]. Despite the considerable need for aerogels, there are limited types of materials that can actually be transformed into an aerogel structure. These include metal oxide aerogels (SiO_2, Al_2O_3, TiO_2) [10–13], carbon material aerogels (carbon, carbon nanotubes, graphene) [10, 14–16], semiconducting chalcogenide aerogels (CdS, CdSe, PbTe) [10, 17, 18], and, more recently, polysaccharide [19] or protein-based aerogels [20]. With advancements in nanotechnology, more-sophisticated preparation strategies are being pursued to create new aerogel materials.

Commonly metal oxide aerogels have been synthesized by a sol–gel process following supercritical drying or frozen drying. In the first step, metal oxide hydrogels are prepared by the sol–gel method; i.e., they are formed in a polymerization process occurring between the metallic atoms M of the

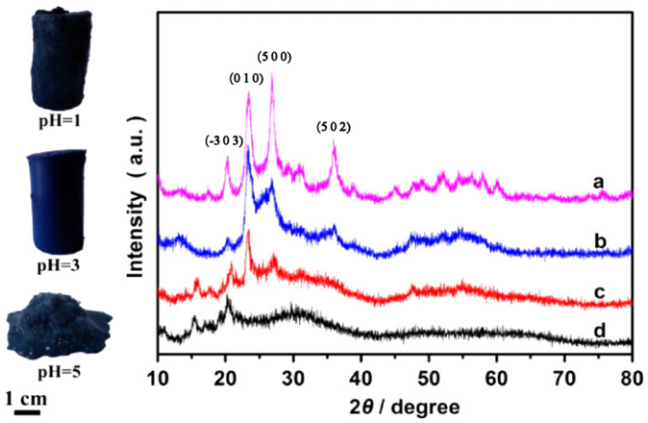

Figure 1. (Left) Optical image of tungsten oxides obtained at different pH values in the hydrothermal process. (Right) XRD patterns of tungsten oxides obtained at different pH values after freeze-drying (a, pH = 1; b, pH = 3; c, pH = 5; d, pH = 9).

precursor molecules by the establishment of M–OH–M or M–O bridges. Then, after supercritical drying or frozen drying, the obtained hydrogels are transformed into aerogels. In this paper, tungsten oxide hydrogel was prepared by a simple hydrothermal process, which can reduce reaction time and enhance the degree of polymerization compared with the sol–gel method. The obtained hydrogel was freeze-dried to produce aerogels, which are non-stoichiometric $W_{18}O_{49}$ consisting of interconnected nanowires. The as-prepared aerogel is very different from the majority of tungsten-oxide aerogels reported in the literature, which are WO_x-containing composites composed of nanoparticles [21, 22]. The as-synthesized tungsten oxides were explored for a direct electrochemistry-based biosensor by immobilization of glucose oxidase (GOD). In comparison with the materials obtained with different pH values, GOD immobilized in tungsten oxide formed at pH = 3 shows more facile direct electrochemistry and better electrocatalytic performance without any electron mediator in the glucose biosensor.

2. Experiments

2.1. Chemicals

Hydrochloric acid ($Na_2WO_4{\cdot}2H_2O$) was purchased from ChuanDong Chemical Reagent Co., (Chongqing, China). D (+) glucose was purchased from DingGuo Biological Technology Co., Ltd (Shanghai, China). Polyethyleneimine (PEI), glucose oxidase (GOD), and Nafion were purchased from Sigma-Aldrich. Phosphate buffer solutions (PBSs) were prepared with 0.1 M of NaH_2PO_4 and 0.1 M of Na_2HPO_4. All chemicals were used as received without any further purification. Distilled water was used in all experiments.

2.2. Synthesis of materials

2.2.1. Synthesis of tungstic acid. 30 g of $Na_2WO_4{\cdot}2H_2O$ was dissolved in 250 mL of deionized water to form a transparent solution, and then hydrochloric acid (6 M) was dropped into the solution under stirring until the pH value of the solution was lower than 1. A yellow precipitate was formed after this acidification process. The product was filtrated and washed several times with deionized water and then oven-dried in air at 50 °C.

2.2.2. Synthesis of tungsten oxide aerogel. 2.5 g of the aforementioned tungstic acid was dispersed into 20 mL of deionized water. This tungstic acid suspension was then added to 2.5 g of 50 wt% PEI aqueous solution. Subsequently, the mixture was diluted with water to 35 mL and its pH value was adjusted to 3 by hydrochloric acid (6 M) under stirring; the mixture was transferred into a 50 mL Teflon-lined stainless steel autoclave and heated at 210 °C for 24 h. After the mixture cooled to room temperature, the sample was taken out and dehydrated by freeze drying. For comparison, tungsten oxide was also synthesized following the same procedure and adjusted to different pH values.

2.3. Physical characterization

The crystal structure of the materials was characterized by powder x-ray diffraction (XRD, XRD-7000). The morphology and microstructure of the synthesized materials were investigated by field emission scanning electron microscopy (FESEM, 7800 F, Japan) and transmission electron microscopy (TEM, JEM-2100).

2.4. Electrochemical measurement

GOD immobilization was achieved by immersing 1 mg of the tungsten oxide ($W_{18}O_{49}$) prepared earlier in 0.1 mL of GOD solution (10 mg · mL^{-1}, pH = 7.4, 0.1 M PBS) under ambient conditions and shaken for 20 min, and then stored at 4 °C for 1 day for protein adsorption. A glass–carbon electrode (GCE) 3 mm in diameter was polished with 0.3 and 0.05 mm of alumina powder, followed by thorough rinsing with deionized water and slight sonication in deionized water. Subsequently, the electrode was modified with chitosan by electrodeposition in a 0.2% chitosan solution at −2.5 V for a few seconds to form a positively charged surface. The bioconjugates previously obtained were re-shaken, and 5 μL of this suspension was deposited on the center of the pre-treated GCE. It was then left to dry at room temperature, after which 10 μL of 0.5% Nafion was subsequently placed on the entire electrode surface to form a Nafion membrane, which was used to fix the GOD-impregnated $W_{18}O_{49}$ materials. The electrochemical measurements were carried out using a three-electrode system, which employed a platinum wire as the counter electrode, a saturated calomel electrode (SCE) as the reference, and a $W_{18}O_{49}$-modified GCE as the working electrode.

3. Results and discussion

During the hydrothermal process, 3D self-assembled samples with cylindrical morphology were obtained at pH of 1 and 3,

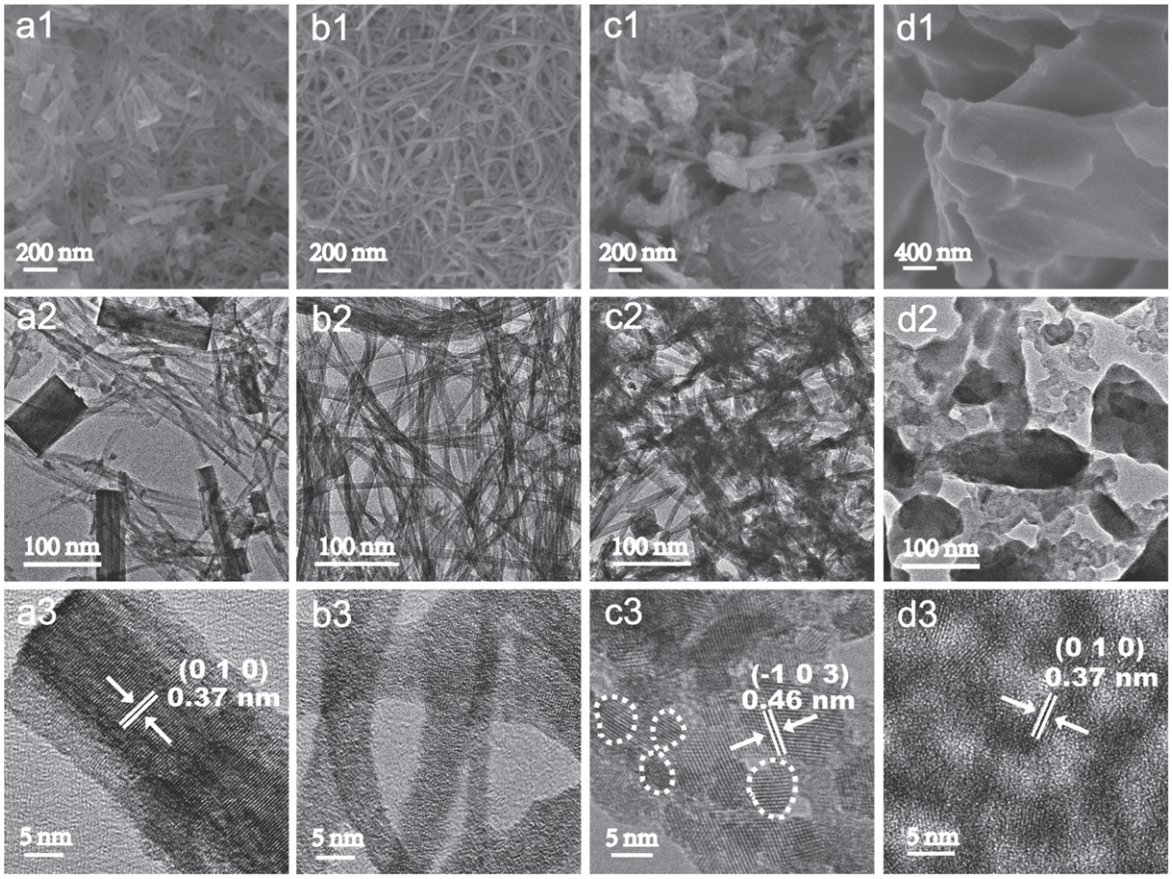

Figure 2. SEM, TEM, and HRTEM images of samples (a1, b1, c1, and d1 are SEM of products obtained at pH = 1, 3, 5, and 9, respectively; a2–3, b2–3, c2–3, and d2–3 are TEM of products obtained at pH = 1, 3, 5, and 9 with different magnification, respectively).

whereas only some watery precipitates were collected when the pH value was higher than 5 (left side of figure 1). After freeze-casting, the obtained samples were first checked by XRD. As can be seen in figure 1, all the main peaks appearing at 20.3°, 23.4°, 26.8°, and 36.0° of the samples obtained with pH equal to 1 and 3 can be indexed undisputedly to the monoclinic $W_{18}O_{49}$ phase [JCPDS No.05-0392], which corresponds to (−303), (010), (500), and (502), respectively. As the pH value of the solution increased, the XRD of these products displayed pronounced diffraction peak broadening. This occurred due to the size of the crystal particles, and high pH favors the formation of tungsten oxides of smaller size. The average crystal particle size of the samples obtained at pH = 1, 3, 5, and 9 was 13.0, 9.8, 8.8, and 2.4 nm, respectively, as estimated by the Scherrer equation. Judging from the intensity of the peaks, the sample synthesized at pH 1 had the best crystallinity. The crystallinity of the final products decreased as the reaction pH value increased. Furthermore, the peak intensity of the (500) plane ($2\theta = 27°$) decreased sharply, which indicates that pH value has a significant effect on the growth of the (500) plane.

The prepared products were further examined by FESEM and TEM. As presented in figures 2(a1)–(d2), the microstructure and morphology of the products synthesized with different pH are very distinctive. The product obtained from pH = 1 (figures 2(a1) and (a2)) was constructed by many short bulky rods (d = 20–100 nm) and long thin wires (about 5 nm in diameter). Interestingly, the aerogels formed at pH = 3 were assembled by ∼5 nm uniform ultrafine nanowires (figures 2(b1)–(b3)). Compared with the tungsten oxide nanowires which have been reported [1], the diameter of the product with pH 3 is finer, whereas the dimension distribution is wider with pH 1. When the pH of the solution increased to 5, some nanoparticles appeared in the products and tangled with the nanowires. With further increase in the solution's pH to 9, the nanowires disappeared completely, and irregular blocks composed of nanoparticles became the dominant products. After a review of the HRTEM results, it was discovered that the materials obtained at higher pH values had a smaller particle size, which is in agreement with the XRD results.

The formation of many very different microstructures by simply changing the solution's pH raises much curiosity. To understand the formation mechanism of the various microstructured samples, the experiments were also conducted under different pH values without using PEI.

As shown in scheme 1, the tungsten acid precursor used in this work has random disklike morphology with a mean thickness of ∼60 nm. After hydrothermal treatment within a pH range of 1 to 5, the products still display disklike morphology but have a well-developed polygon shape with a flake structure. At a pH of 9, the products consist of large

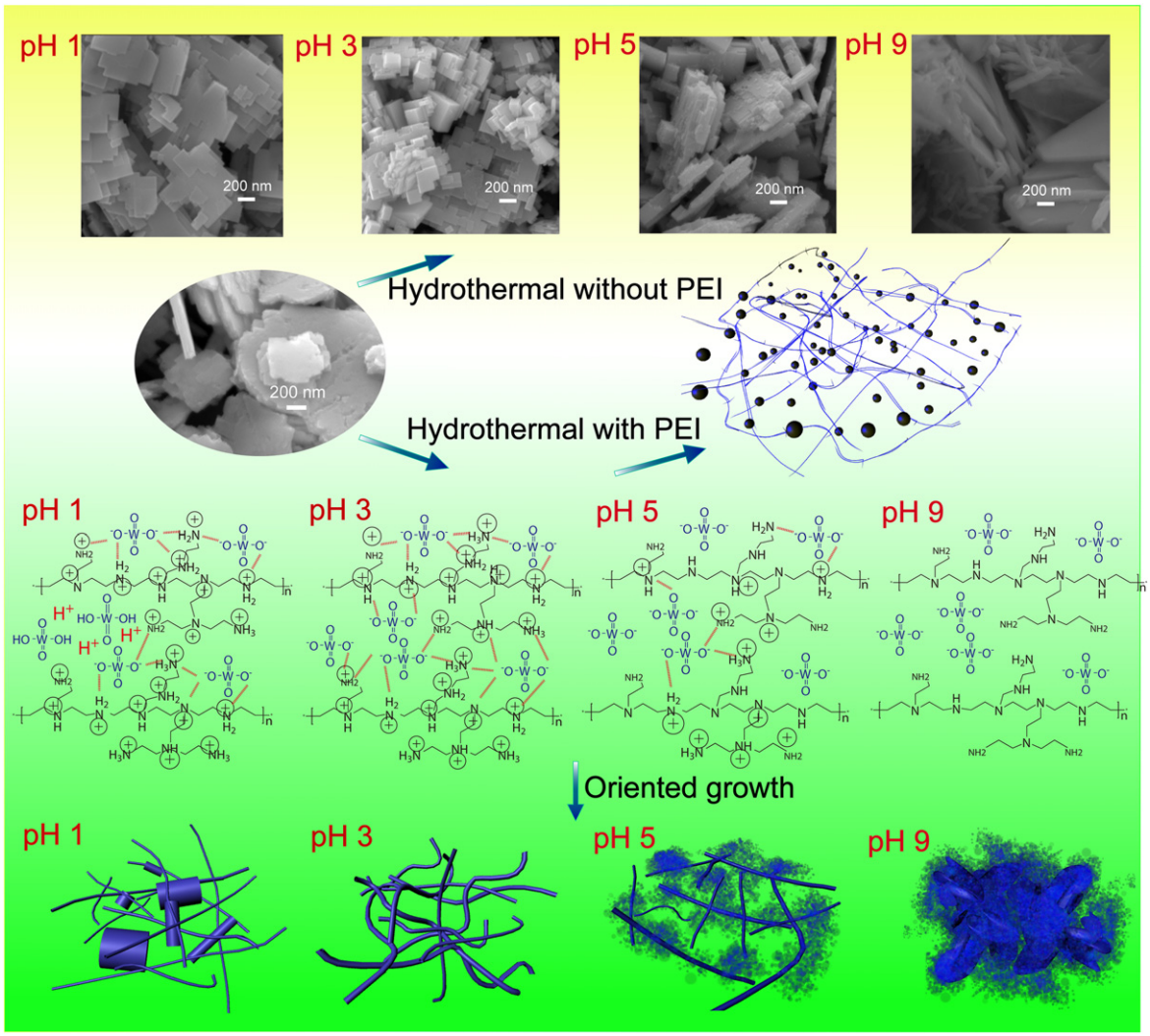

Scheme 1. Schematic illustrations showing the mechanism of tungsten oxide-oriented growth (SEM images above and diagram below).

disklike flakes and small nanorods; however, the yield is far less than that of the other three samples. By comparing the SEM images of the samples obtained in different conditions, it is found that the PEI plays an important role in controlling the morphology of products. Linear PEI is a water-soluble polycation polymer with high ionic charge density, meaning that it has a very strong affinity with anionic materials like polyanions and negatively charged solids. Based on other literature, the protonation degree of PEI is strongly dependent on the pH value of the solution in question. At a pH lower than 3, at least 90% of PEI protonation occurs. When the pH increases, the protonation degree decreases greatly, and at a pH of 9, the protonation degree can reach only about 20% [23]. Hence, as demonstrated in scheme 1, when tungstic acid is added to the PEI solution under high temperatures in the hydrothermal process, negatively charged tungsten acid radicals are generated and can be easily adsorbed by the

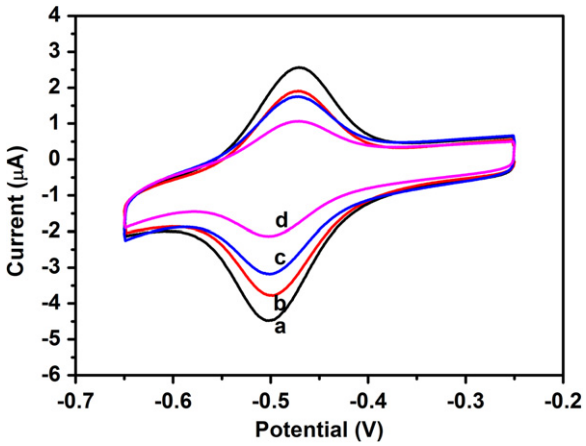

Figure 3. CVs of the GOD-different tungsten oxide–modified electrodes in pH 7.4 nitrogen–saturated PBS (tungsten oxide synthesized at pH 1 (b), pH 3 (a), pH 5 (c), and pH 9 (d)).

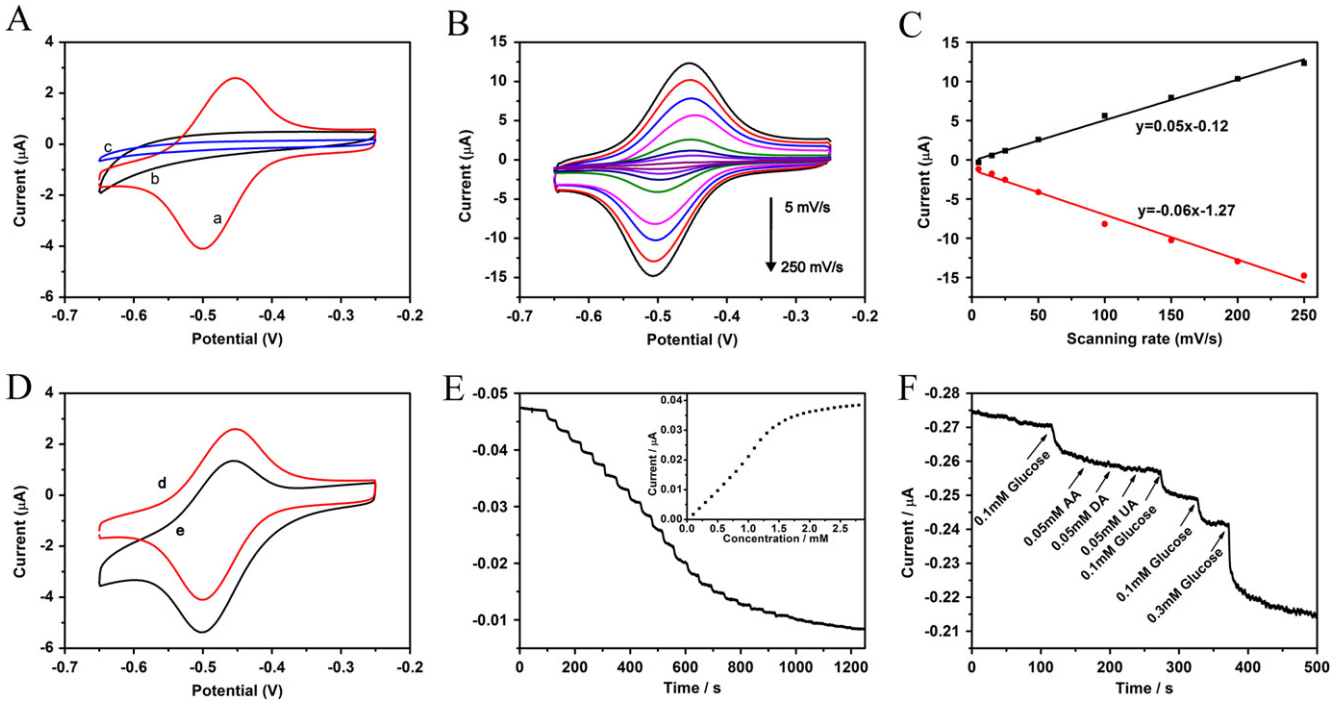

Figure 4. (a) Cyclic voltammograms of different electrodes in N_2-saturated 0.1 M PBS. The letters a, b, and c stand for the CV of the electrode, which is modified by Nafion/GOD/$W_{18}O_{49}$, Nafion/$W_{18}O_{49}$, and Nafion/GOD, respectively. (b) Cyclic voltammograms of Nafion/GOD/$W_{18}O_{49}$-modified GCE in 0.1 M of PBS solution at different scan rates (from 5 to 250 mV s^{-1}, inside to outside). (c) Plots of peak currents versus scan rate. (d) Cyclic voltammograms of Nafion/GOD/$W_{18}O_{49}$-modified GCE in air-saturated (letter e) and N_2-saturated (letter d) PBS at 50 mV s^{-1}. (e) Typical steady-state response of the biosensor upon successive injections of 1 μmol of glucose solution into 10 ml of 0. 1 M PBS at −0.45 V. The inset is the calibration curve of the sensor. (f) Effect of the interfering species on the biosensor response.

ammonium sites of the PEI. The surface of PEI provides a site for tungstic acid nucleation, recrystallization, and eventually dehydration to form tungsten oxide. In addition, the adsorption process is largely governed by the protonation degree of the PEI and the concentration of negatively charged tungsten acid radicals, which result in different morphology. When the pH value increases, tungstic acid reacts in part with hydroxyl, and the interaction between the negatively charged tungsten acid radicals and the PEI weakens gradually. A 3D continuous network structure fails to fully develop, so the product contains some blue precipitation instead of a hydrogel column.

For a long time, the bioelectrocatalytic oxidation of glucose has been the focus of much investigation. Its importance stems from its potential use in sensing sugar in human blood and also in biofuel cell applications. In this work, GOD was used as an example to demonstrate the bioelectrocatalytic application of tungsten oxide aerogels as electrode modification materials. To investigate the bioactivity of adsorbed protein, the fabricated electrodes were employed as a biosensor for glucose electrochemical oxidation. Figure 3 shows the cyclic voltammograms (CVs) of the GOD-different tungsten oxide–modified electrodes. The GOD immobilized on tungsten oxide formed at pH = 3 displayed the strongest redox peaks. The results indicate that the unique 3D network structure consisting of uniform ultrafine nanowires is beneficial for immobilizing bio-enzymes and can help GOD to achieve direct electron transfer. So the material obtained at pH 3 was chosen for further detection of glucose.

Figure 4(a) shows the cyclic voltammograms of different electrodes prepared under the same conditions in 0.1 M of pH 7.4 nitrogen–saturated PBS solution at 50 mV s^{-1}. A pair of well-defined redox peaks were observed for the Nafion/GOD/$W_{18}O_{49}$-modified GCE (curve a), but no obvious redox peaks for either $W_{18}O_{49}$-modified or GOD-alone-modified electrodes (curves b and c), which suggested that the Nafion/GOD/$W_{18}O_{49}$-modified GCE clearly demonstrated direct electron transfer capability. The effect of the scan rate on the electrochemical response of the immobilized GOD is displayed in figures 4(b) and (c). The redox peak current increases linearly with the increase in the scan rate from 5 to 250 mV s^{-1}, which indicates that the GOD redox reaction is a surface-controlled electrochemical process. The peak-to-peak separation of the CVs increases with the increase in the scan rate due to the resistance of the modified layer [24]. Figure 4(d) displays the cyclic voltammograms of the Nafion/GOD/$W_{18}O_{49}$-modified GCE in N_2- and air-saturated 0.1 M PBS solution. A pair of well-resolved redox peaks can be observed in both the N_2- and the air-saturated PBS. In the presence of oxygen, the reduced enzyme (GOD-$FADH_2$) can be further oxidized by dissolved oxygen very quickly at the surface of the electrode, as in the following [25]:

$$GOD - FADH_2 + O_2 \rightarrow GOD - FAD + H_2O_2$$

Figure 4(e) shows a typical current–time plot for the Nafion/GOD/$W_{18}O_{49}$ GCE with successive injections of a glucose solution into 0.1 M pH 7.4 PBS solutions at −0.45 V. Each successive increase of 0.1 mmol L^{-1} of glucose results

in a decrease in the steady-state current, which shows a sensitivity of 2.69×10^{-4} mA mmol^{-1} cm^{-2} and a fast response of about 10 s (figure 4(b)). The calibration curve of the electrode (inset of figure 4(b)) shows a linear response range from 0.01 mM to 1.0 mM, with a correlation coefficient of 0.999. The biosensor also shows good selectivity for glucose (figure 4(f)). In a PBS solution that contains 0.1 mM of glucose, there is no significant change in the amperometric response owing to the addition of 0.05 mM of AA, DA, and UA. Additional injections of 0.1 mM and 0.3 mM of glucose confirm that the sensor maintains performance in the presence of the interfering species. The sensor modified by $W_{18}O_{49}$ aerogel shows a lower detection limit (10 μM) and a similar response time (10 s) compared with other nano metal oxides of ZnO and TiO_2 [24, 26].

4. Conclusions

In summary, a tungsten oxide aerogel with a unique 3D network consisting of uniform ultrafine nanowires was fabricated by a PEI-assisted hydrothermal method. Following comparison of the experimental results in the presence of PEI and without PEI at different pH, a reasonable formation mechanism for tungsten oxide aerogel was proposed. The $W_{18}O_{49}$ aerogel obtained at pH = 3 showed excellent sensing performance in terms of high sensitivity, low detection limit, and fast response based on the direct electrochemistry of GOD. Our work not only provides an effective route for preparing metallic oxide aerogels but also provides a good example of broadening the application of tungsten oxides.

Acknowledgments

This work is financially supported by the National Natural Science Foundation of China (21163021 and 21375108); the Chongqing Key Laboratory for Advanced Materials and Technologies of Clean Energies, Institute for Clean Energy & Advanced Materials (Southwest University, Chongqing, China); a start-up grant under SWU111071 & SWU113077 from Southwest University and Chongqing Science and Technology Commission under cstc2011pt-sy90001 and cstc2012gjhz90002 (Chongqing, China); the Natural Science Foundation of Chongqing (cstc2013jcyjA5004); Fundamental Research Funds for the Central Universities (XDJK2013B031).

References

[1] Li X-L, Liu J-F and Li Y-D 2003 Large-scale synthesis of tungsten oxide nanowires with high aspect ratio *Inorg. Chem.* **42** 921–4
[2] Li X-L, Lou T-J, Sun X-M and Li Y-D 2004 Highly sensitive WO_3 hollow-sphere gas sensors *Inorg. Chem.* **43** 5442–9
[3] Zhou H, Shi Y, Wang L, Zhang H, Zhao C, Hagfeldt A and Ma T 2013 Notable catalytic activity of oxygen-vacancy-rich $WO_{2.72}$ nanorod bundles as counter electrodes for dye-sensitized solar cells *Chemical Communications* **49** 7626–8
[4] Cheng L, Hou Y, Zhang B, Yang S, Guo J W, Wu L and Yang H G 2013 Hydrogen-treated commercial WO_3 as an efficient electrocatalyst for triiodide reduction in dye-sensitized solar cells *Chemical Communications* **49** 5945–7
[5] Zheng H, Ou J Z, Strano M S, Kaner R B, Mitchell A and Kalantar-zadeh K 2011 Nanostructured tungsten oxide–properties, synthesis, and applications *Advanced Functional Materials* **21** 2175–96
[6] Pol S, Pol V, Kessler V, Seisenbaeva G, Solovyov L and Gedanken A 2005 Synthesis of WO_3 nanorods by reacting $WO(OMe)_4$ under autogenic pressure at elevated temperature followed by annealing *Inorg. Chem.* **44** 9938–45
[7] Kettunen M, Silvennoinen R J, Houbenov N, Nykänen A, Ruokolainen J, Sainio J, Pore V, Kemell M, Ankerfors M and Lindström T 2011 Photoswitchable superabsorbency based on nanocellulose aerogels *Advanced Functional Materials* **21** 510–7
[8] Chen X, Zhou Y, Liu Q, Li Z, Liu J and Zou Z 2012 Ultrathin, single-crystal WO_3 nanosheets by two-dimensional oriented attachment toward enhanced photocatalystic reduction of CO_2 into hydrocarbon fuels under visible light *ACS Applied Materials & Interfaces* **4** 3372–7
[9] Huang J, Xu X, Gu C, Yang M, Yang M and Liu J 2011 Large-scale synthesis of hydrated tungsten oxide 3D architectures by a simple chemical solution route and their gas-sensing properties *J. Mater. Chem.* **21** 13283–9
[10] Jung S M, Jung H Y, Dresselhaus M S, Jung Y J and Kong J 2012 A facile route for 3D aerogels from nanostructured 1D and 2D materials *Scientific Reports* **2** 849
[11] Baumann T F, Gash A E, Chinn S C, Sawvel A M, Maxwell R S and Satcher J H 2005 Synthesis of high-surface-area alumina aerogels without the use of alkoxide precursors *Chem. Mater.* **17** 395–401
[12] Moner-Girona M, Roig A, Molins E and Llibre J 2003 Sol-gel route to direct formation of silica aerogel microparticles using supercritical solvents *J. Sol-Gel Sci. Technol.* **26** 645–9
[13] Baia L, Peter A, Cosoveanu V, Indrea E, Baia M, Popp J and Danciu V 2006 Synthesis and nanostructural characterization of TiO_2 aerogels for photovoltaic devices *Thin Solid Films* **511** 512–6
[14] Horikawa T, Hayashi J I and Muroyama K 2004 Size control and characterization of spherical carbon aerogel particles from resorcinol–formaldehyde resin *Carbon* **42** 169–75
[15] Worsley M A, Satcher J H Jr and Baumann T F 2008 Synthesis and characterization of monolithic carbon aerogel nanocomposites containing double-walled carbon nanotubes *Langmuir* **24** 9763–6
[16] Worsley M A, Pauzauskie P J, Olson T Y, Biener J, Satcher J H Jr and Baumann T F 2010 Synthesis of graphene aerogel with high electrical conductivity *J. Am. Chem. Soc.* **132** 14067–9
[17] Mohanan J L, Arachchige I U and Brock S L 2005 Porous semiconductor chalcogenide aerogels *Science* **307** 397–400
[18] Bag S, Trikalitis P N, Chupas P J, Armatas G S and Kanatzidis M G 2007 Porous semiconducting gels and aerogels from chalcogenide clusters *Science* **317** 490–3
[19] García-González C, Alnaief M and Smirnova I 2011 Polysaccharide-based aerogels—Promising biodegradable carriers for drug delivery systems *Carbohydrate Polymers* **86** 1425–38
[20] Betz M, García-González C, Subrahmanyam R, Smirnova I and Kulozik U 2012 Preparation of novel whey protein-based aerogels as drug carriers for life science applications *J. Supercritical Fluids* **72** 111–9

[21] Li X, Yang S, Sun J, He P, Xu X and Ding G 2014 Tungsten oxide nanowire-reduced graphene oxide aerogel for high-efficiency visible light photocatalysis *Carbon* **78** 38–48

[22] Moreno-Castilla C, Maldonado-Hodar F J, Rivera-Utrilla J and Rodriguez-Castellon E 1999 Group 6 metal oxide-carbon aerogels. Their synthesis, characterization and catalytic activity in the skeletal isomerization of 1-butene *Appl. Catalysis* A **183** 345–56

[23] Chen C-C and Kuo P-L 2006 Gold nanoparticles prepared using polyethylenimine adsorbed onto montmorillonite *J. Colloid Interface Sci.* **293** 101–7

[24] Bao S-J, Li C M, Zang J-F, Cui X-Q, Qiao Y and Guo J 2008 New nanostructured TiO_2 for direct electrochemistry and glucose sensor applications *Advanced Functional Materials* **18** 591–9

[25] Liu S Q and Ju H X 2003 Reagentless glucose biosensor based on direct electron transfer of glucose oxidase immobilized on colloidal gold modified carbon paste electrode *Biosens. Bioelectron.* **19** 177–83

[26] Wang J X, Sun X W, Wei A, Lei Y, Cai X P, Li C M and Dong Z L 2006 Zinc oxide nanocomb biosensor for glucose detection *Appl. Phys. Lett.* **88** 233106